A Strength Based Criterion for the Prediction of Stable Fibre Crack-Bridging

J.A. Bennett, R.J. Young

A Strength Based Criterion for the Prediction of Stable Fibre Crack-Bridging

J.A. Bennett, R.J. Young

PII: S0266-3538(07)00483-6
DOI: 10.1016/j.compscitech.2007.12.010
Reference: CSTE 3932

To appear in: *Composites Science and Technology*

Received Date: 9 November 2006
Revised Date: 8 December 2007
Accepted Date: 10 December 2007

Please cite this article as: Bennett, J.A., Young, R.J., A Strength Based Criterion for the Prediction of Stable Fibre Crack-Bridging, *Composites Science and Technology* (2007), doi: 10.1016/j.compscitech.2007.12.010

A Strength Based Criterion for the Prediction of Stable Fibre Crack-Bridging

J. A. Bennett and R. J. Young*

Northwest Composites Centre, School of Materials, University of Manchester, Grosvenor Street, Manchester, M1 7HS, UK

Abstract

The likelihood that a fibre will form a stable bridge across a propagating crack has been investigated by means of experimental measurements and the theoretical consideration of the balance between interfacial strength, fibre strength, the physical properties of the component materials and the stress transfer characteristics of bonded and debonded interfaces. A simple strength based criterion has been developed from traditional stress transfer models to predict if a fibre will form a stable bridge across a propagating matrix crack. The first step in the analysis takes into consideration a range of stress transfer parameters to predict whether the build up of stress caused by the matrix crack is sufficient for the fibre to fracture or if it will cause debonding from the surrounding matrix. This is then extended to include the subsequent build up of stress in the case where the fibre debonds from the matrix. The criterion is compared to experimental data for a range of fibre/matrix systems. Raman spectroscopy was used to measure the point to point distribution of fibre strain along Twaron, Zylon, T50u and M5 fibres embedded in an epoxy resin matrix and lying perpendicular to a matrix crack. The experimental data showed that while some fibres debonded partly from the matrix and formed a stable bridge, others fractured with only a small amount of debonding.

Keywords: A. Polymer-matrix composites; B. Fracture; C. Fibre bridging; D. Raman spectroscopy;

*Corresponding author
email: robert.young@manchester.ac.uk
Tel : +44-161-306-3551
Fax : +44-161-306-8840

1 Introduction

When a stressed material fails by fracture, the opening of the resultant crack is opposed by the fracture resistance of the material. This resistance may be attributed to mechanisms that absorb and/or dissipate energy. When considered in the context of fibre reinforced composites it has been shown that enhanced toughness requires that a matrix crack leaves intact fibres in its wake to act as a restraint across the faces of the crack. Crack bridging, fibre fracture, interfacial-debonding and fibre sliding significantly affect the resistance to crack propagation and hence toughness of the material [1-3]. These processes, however, are all interlinked and the significance of one may depend upon the characteristics of another, for instance if the advancing crack causes immediate fibre fracture then although energy has been used in breaking the fibre there can be no crack bridging or interfacial debonding and hence no fibre sliding.

The tendency of a matrix crack to deflect along the fibre/matrix interface has been observed experimentally and has been shown theoretically to be dependent on the degree of mismatch between the elastic properties of the two materials [4]. Bennett and Young [5] have observed fibre/crack interactions in aramid epoxy composites and noted for fibres ahead of the crack tip that the fibre strain distribution indicated interfacial failure when using untreated (weak interface) fibres in contrast to the behaviour of surface-activated (strong interface) fibres which remained fully bonded. It was noted, however, that debonding occurred in the crack bridging fibres for both types of fibre, although it was found that further propagation of the debond was more difficult in composites made with surface-activated fibres.

In the case of a semi-infinite matrix crack normal to the direction of the fibre axis and loaded symmetrically about the crack plane, that has impinged upon and advanced slightly beyond an embedded fibre, but for which no fibre/matrix debonding has occurred, two outcomes are envisaged [1]:-

a) Fibre/matrix debonding occurs and a mode II crack deflects along the fibre/matrix interface with no fibre fracture
b) No debonding occurs and fracture of the fibre occurs when it is loaded beyond its ultimate tensile strength ($_f^*$).

In this study an effort is made to understand why matrix crack propagation causes some fibres to simply fracture, while others exhibit a degree of debonding from the matrix before subsequent fracture. This is done by establishing a link between conventional strength based theory [6-9], micromechanical considerations and experimental data obtained using Raman

spectroscopy to follow the deformation micromechanics of the fibre/matrix interface in model composites where a matrix crack has been propagated.

2 Criterion for interfacial failure

2.1 Fully-bonded case

As a starting point, a matrix crack is assumed to have propagated normal to and beyond an embedded fibre, of uniform strength causing no damage to the fibre in the process. Further, the matrix crack is spanned by the unbroken fibre and no debonding has taken place.

The application of load to a fibre, in this case by crack opening, in order to extract it from the matrix by a 'pull-out' process, results in a stress distribution along the region of the fibre embedded within the matrix [10]. The shear lag model [11] that has been used extensively for analysis of stress distributions in pull-out/crack-bridging tests, can be used to describe the build up and transfer of fibre stress, $_f$, from the point where the fibre enters the resin to some point along the fibre axis where the tensile stress has decayed to zero. Failure of the fibre/matrix interface occurs when the interfacial shear strength, $_{max}$, is reached. The conditions which determine the likelihood of fibre/matrix interfacial failure occurring instead of fibre fracture, can be examined using the shear lag model. The shear lag distribution of strain, along a fully bonded fibre can be described by [11],

$$e_{app} = e_f \frac{\sinh[n(L_e - x/r]}{\sinh(ns)} \tag{1}$$

where e_{app} is the strain acting on the fibre outside the matrix, e_f is the fibre strain at a distance x inside the matrix, L_e is the embedded length, r is the fibre radius, s is the fibre aspect ratio (L_e/r). The Cox analysis gave a value of n in terms of fibre and matrix properties, but recent shear-lag analyses [12-14] have shown it to be inaccurate. The n parameter used here is based on the parameter derived correctly by Nairn [12], where $n = r$ [10] such that

$$n^2 = \frac{2}{E_f E_m}\left[\frac{E_f V_f + E_m V_m}{V_m/(4G_f) + 1/(2G_m)\left((1/V_m)\ln(1/V_f) - 1 - (V_m/2)\right)}\right] \tag{2}$$

E_f and G_f are the fibre Young's and shear moduli, E_m and G_m are the matrix Young's and shear moduli and r is the fibre radius. V_f is the fibre volume fraction and V_m is the volume fraction of matrix, such that if R is the cylinder of surrounding matrix then $V_f = r^2/R^2$ and V_m

$= (R^2 - r^2)/R^2$. The fibre strain is a maximum at the crack plane ($x = 0$) where the fibre enters the matrix. Following work by Cervenka *et al* [15] values of R used in this study reflect n values obtained by fitting the shear lag model to experimental data obtained from Raman strain mapping experiments on model composites. Similarly the corresponding interfacial shear stress, , at a distance x along the interface, given by

$$\tau = \frac{n}{2} E_f e_{app} \frac{\cosh[n(L_e - x)/r]}{\sinh[ns]} \quad (3)$$

is a maximum at the crack plane ($x = 0$). Since both the interfacial shear stress and the stress acting on the fibre, are a maximum at the crack-plane then failure should be expected to initiate from this point. For fibre aspect ratios > 15, applying the condition $x = 0$ to *equation 3* gives

$$\tau = \frac{n}{2} E_f e_f \quad (4)$$

If the fibre deforms in an elastic manner (according to Hooke's Law) then,

$$\tau = \frac{n}{2} \sigma_f \quad (5)$$

where $_f$ is the fibre stress. If fibre fracture occurs when the stress in the fibre reaches its ultimate tensile strength, $_f^*$, then setting the boundary condition at

$$\sigma_f = \sigma_f^* \quad (6)$$

and substituting into *equation 5* gives a relationship between the strength of the fibre and the interfacial shear stress such that if

$$\sigma_f^* < \frac{2\tau}{n} \quad (7)$$

then the *fibre will fracture*. Similarly if interfacial debonding/yielding is considered to occur when the interfacial shear stress reaches its shear strength

$$\tau = \tau_{max} \quad (8)$$

then by substituting *equation 8* into *equation 5* a boundary condition for fibre/matrix interfacial failure can be established whereby,

$$\tau_{max} < \frac{n c_f}{2} \quad (9)$$

This approach suggests that the outcome of a matrix crack impinging on an embedded fibre depends on the balance between the fibre strength and the shear strength of the

interface. If $_{max}$ is known then it is also possible to define a critical ratio of fibre strength to fibre modulus by substituting *equation 2* into *equation 9* and rearranging to give

$$\frac{\sigma_f{}^{*2}}{E_f} > a\tau_{max}^2 \tag{10}$$

where *a* is constant and a function of the geometric and matrix of the material parameters only given by

$$a = 2E_m\left[\frac{V_m/(4G_f)+1/(2G_m)((1/V_m)\ln(1/V_f)-1-(V_m/2))}{E_fV_f+E_mV_m}\right] \tag{11}$$

Lines that demonstrate the calculated relationship between $_f^*$ and E_f are shown in *figure 1.* Plotting $_f^*$ against $E_f^{1/2}$ for the above condition according to *equation 10* defines the boundary between interfacial failure and fibre failure. It can be seen from *figure 1* that for any given set of stress transfer conditions, if the fibre modulus increases then there is a greater tendency for fibre fracture. Conversely if the fibre strength increases then the balance shifts towards interfacial failure.

2.1.1. Effect of interfacial shear strength

The interfacial bonding between a fibre and matrix system can be altered by the application of physical or chemical fibre surface treatments [16]. Any change in the interfacial shear strength, $_{max}$, of a fibre/matrix system will influence the crack-bridging capabilities of the fibre and consequently the toughening or structural properties of the material. *Figure 1a* shows the theoretical boundary conditions drawn at several levels of interfacial strength, $_{max}$, for a system with a matrix of modulus, E_m = 3 GPa and Poissons ratio, $_m$ = 0.35, incorporating a fibre of radius, r = 6.25 m. The interfacial geometric parameter n was set at 0.1. It can be seen that as the interfacial shear strength, $_{max}$, is increased from 20 MPa to 60 MPa, through an improvement in interface strength, the balance between interfacial failure and fibre fracture shifts towards fibre fracture. Thus in a system with a high interfacial shear strength, fibre fracture will be more likely then for a system with low interfacial shear strength. The maximum recorded value of interfacial shear strength for the systems studied here, 43 MPa, is close to the shear yield stress of the matrix [8] and could represent interfacial failure by either matrix yielding or fibre/matrix debonding.

2.1.2 Effect of shear lag fitting parameter n

The fibre shear lag fitting parameter n also has an effect on the boundary between fibre fracture and interfacial failure. If the parameters are as above with both matrix modulus, E_m, and interfacial shear strength, $_{max}$, are kept constant at 3 GPa and 40 MPa respectively, then it can be seen from *figure 1b* that changing the value of n has a significant effect. As the value of n is decreased from 0.1 to 0.08 then it can be seen that the boundary shifts in favour of fibre fracture.

2.2 Partially-debonded case

In many fibre/matrix systems the propagation of a primary matrix crack will lead to debonding in the form of a mode II crack propagating along the fibre/matrix interface over part of the fibre embedded length. The strain distribution in this case can be described by a combination of

$$e_f = \frac{2\tau x}{r E_f} \tag{12}$$

in the debonded region, where x is the distance long the fibre, and *equation 1* in the bonded region.

Consideration of the theoretical strength criterion for crack-bridging can be extended to account for propagation of interfacial failure. Once debonding has been initiated, if the fibre properties are uniform along its length and debonding causes no damage to the fibre, then the fibre sliding is opposed by friction alone. Further crack-opening will cause debonding to propagate along the fibre/matrix interface. In this case two components of the micromechanical stress distribution must be considered, the lower strain elastic bonded region and the higher strain debonded region. The limiting value of interfacial shear strength, which is encountered at the beginning of the bonded region must be continually overcome for further failure of the fibre/matrix bond and hence debond propagation. In addition the transfer of interfacial frictional shear stress causes a build up of axial fibre stress in the debonded region, which is a maximum at the crack-plane. As a consequence of the build up of frictional shear stress, it is inevitable that as debonding proceeds the axial fibre stress will reach the tensile strength of the fibre.

Debonding along a continuous fibre is assumed to proceed in a stable manner, at a constant shear stress, τ_{max}, and a constant fibre stress, σ_f, at the point of debonded/bonded transition, $x = L_d$. As the debond crack advances, the maximum value of interfacial shear stress is always found where the strain gradient is greatest; this has been shown to be at the debonded/bonded transition [6]. Generally, frictional stress transfer in the debonded region causes an increase in the axial fibre stress which tends towards the tensile strength of the fibre, σ_f^*. However, one case where this does not apply is for an interfacial frictional shear stress of zero, where debonding would continue unchecked over the whole of the fibre length.

If partial-debonding conditions are applied, then the overall stress in the fibre is the sum of the stress built up in the debonded and bonded region. This can be written as

$$\sigma_f = \Delta\sigma_{f,d} + \Delta\sigma_{f,b} \tag{13}$$

where $\sigma_{f,d}$ is the build up of stress in the debonded region and $\sigma_{f,b}$ is the build up of stress in the bonded region.

The build up of stress in the debonded region is determined by the rate of change of stress along the fibre and the length of the debonded region L_d, such that

$$\Delta\sigma_{f,d} = \frac{d\sigma_f}{dx} L_d \tag{14}$$

where L_d is the debonded length and $d\sigma_f/dx$ in the debonded region can be found by substituting $\tau_i = \tau_{frict}$ into a stress balance equation [13]

$$\tau = E_f \frac{de_f}{dx} \frac{r}{2} \tag{15}$$

to give

$$\frac{d\sigma_f}{dx} = \frac{2\tau_{frict}}{r} \tag{16}$$

where τ_{frict} is the frictional sliding stress in the debonded region. The build up of stress in the debonded region can be determined by *substituting equation 16* into *equation 14* to give,

$$\Delta\sigma_{f,d} = \frac{2L_d}{r}\tau_{frict} \tag{17}$$

Finally, substituting $\sigma_f = \sigma_f^*$, *equation 5* (for $\tau = \tau_{max}$) and *equation 17* into *equation 13* yields,

$$\sigma_f^* = \frac{2\tau_{max}}{n} + \frac{2L_d}{r}\tau_{frict} \tag{18}$$

which simplifies to,

$$\sigma_f^* = 2\left(\frac{\tau_{max}}{n} + \frac{L_d}{r}\tau_{frict}\right) \quad (19)$$

Plotting $_f^*$ against $E_f^{1/2}$ for the above condition produces curves (*figure 2*) that define the boundary between continuing interfacial failure and fibre fracture along a partially-debonded fibre.

2.2.1 Effect of interfacial frictional shear stress

The interfacial frictional shear stress that can be observed to vary between both systems with different fibre/matrix combinations and systems where the fibre surface has been modified to optimise the level of adhesion, determines the rate at which stress is transferred to the fibre along the debonded length, and hence any change will affect the eventual failure of the crack bridging fibre. *Figure 2a* shows the theoretical boundary conditions drawn at several levels of interfacial frictional shear stress, $_{frict}$, for a partially debonded system with a matrix of modulus, E_m = 3 GPa and Poissons ratio, $_m$ = 0.35, incorporating a fibre of radius, r = 6.25 m. The interfacial geometric parameter n was set at 0.1 and the interfacial shear strength, $_{max}$ = 40 MPa. In the failed/debonded region of the interface, the debond length, L_d, is set at an arbitrary value of 400 m.

2.2.2 Effect of debond length

The length of the failed/debonded interface, L_d, also has an effect on the build up of axial fibre stress. As the length of the failed/debonded region increases then the distance over which the axial fibre stress builds by friction is increased. The effect of this with respect to fibre fracture can be seen in *figure 2b* where the boundary has been drawn for several lengths of interfacial failure/debonding. The parameters used are the same as above, except the interfacial frictional shear stress is kept constant at a typical mean value of 8 MPa. It can be seen that as the distance over which interfacial failure occurs increases from 200 m to 800 m then the fibre strain builds up, moving the balance between fibre fracture and interfacial failure so that fibre fracture becomes more likely.

3 Experimental Procedure

3.1 Materials

The fibres used in this study were a Twaron (PPTA), Zylon (PBO), T50u (carbon) and M5 (PIPD). Each fibre was used in the as-received condition i.e. without removing the manufacturers proprietary sizing or surface finish. The mechanical properties of the fibres are detailed in *Table 1*. The matrix material, a two part, cold-curing epoxy resin from Ciba-Geigy (LY5052/HY5052), has a Young's modulus, $E_m \sim 3$ GPa and a Poisson's ratio, $_m \sim 0.35$.

3.2 Composite Compact Tension (CCT) Specimens

The CCT specimens were prepared using a window-card and a square 'picture-frame' mould. A continuous fibre was mounted across a hole on the window-card. The window-card was then fixed into the mould that was subsequently filled with resin. The mould was then left to cure at room temperature (22 2 C) for a minimum of 7 days. Once cured the 3 mm thick resin sheet was machined into compact tension specimens such that the notch ran perpendicular to the direction of the fibre axis. Two holes of diameter 6 mm were drilled to allow the insertion of pins for loading of the sample as indicated in *figure 3*. The notch was then loaded using a sharp wedge (razor blade) until a sharp matrix crack propagated beyond the fibre.

3.3 Raman Spectroscopy

3.3.1 Single Fibre Deformation in Air

For many high-performance fibres the peak positions of certain Raman bands have been demonstrated to shift to lower wavenumber by the application of tensile stress [5-9]. For all the fibres used in this study there is an approximately linear shift of the peak wavenumber, , with axial fibre strain, e_f. The values of d /de_f used here are listed in *Table 2* [17].

3.3.2 Strain Mapping

The CCT specimen was mounted on a miniature materials straining rig, which was in turn mounted on the microscope stage of the Spex 1000M Raman spectrometer and Raman spectra were obtained from the fibre within the resin using the 632.8 nm red line of a 15 mW helium-neon laser focused to a 5 m spot through the epoxy resin and onto the surface of the fibre. Raman band position profiles were mapped by recording individual spectra in steps of at least 10 m along the crack bridging fibre with the crack open. The deformation needed to open the crack was applied to the sample by the straining rig, at the positions indicated on

figure 3. The COD was recorded as the distance measured (at the sample surface) between the faces of the crack, at a point corresponding to that where the fibre bridged the crack. The profiles of Raman band positions were converted to fibre strain profiles using the shift values in *Table 2*.

3.3 Scanning electron Microscopy

After the Raman investigation the CCT specimens were broken into two pieces along the crack-plane and sputtered with a thin coating of gold. The points at which the fibre had bridged the crack were examined in a Philips XL30 scanning electron microscope with a field emission gun. The microscope was operated at 1kV.

4 Fibre bridging - experimental data

4.1 Twaron

Figure 4a shows the distribution of fibre strain along a Twaron fibre embedded in a crack epoxy resin CCT specimen, derived using measurements of peak shift and the calibration value of the 1610 cm^{-1} Raman band (*Table 2*), for the deformation of Twaron in air. Each point represents the axial fibre strain calculated from a single Raman spectrum. The fibre strain distribution shown in *figure 4a* is for a crack opening displacement (COD) of 12 m, which is the distance between the faces of the crack at the point where it is bridged by the fibre under examination. The point $x = 0$ defines the location of the crack plane; x is positive to the right and negative to the left of the crack plane.

It can be seen that opening of the matrix crack has created a distribution of strain along the fibre to both the right and the left hand side of the crack. The fibre strain, which is maximum at the crack-plane, decays in both directions, tending to zero at some distance, x, along the fibre. The fibre strain distribution (on each side of the crack-plane) can be divided into two regions. The first is a higher strain region with a linear strain gradient, which is characteristic of strain transfer being controlled by friction, hence the fibre is sliding and fibre/matrix debonding has taken place. This region itself can be divided into of two sub-regions, which have different strain gradients, indicating the fibre is subjected to different levels of friction. It can be seen that the fibre has debonded ~ 0.4 mm to the right and ~ 0.4 mm to the left of the crack plane, giving an overall debonded length of ~0.8 mm. The strain in the fibre at the end of these regions is 0.71 % and 0.92 % respectively.

The end of the linear region marks the transition from the debonded to a fully-bonded

region and is characterised by a sharp change in the gradient of the strain profile. The variation of fibre strain in this region is non-linear and shows an exponential decay; this is characteristic of elastic strain transfer, indicating that the fibre and matrix in this region remain bonded. In the bonded region, strain decays and tends towards zero over a distance of ~ 0.5 mm.

The distribution of fibre strain is approximately symmetrical about the crack-plane indicating that the same processes are taking place on either side of the crack-plane. One notable deviation from the symmetrical distribution can be observed to the right hand side of the crack where there is an immediate drop or discontinuity in strain over a distance of x = 0 - 0.1 mm. This phenomenon has been observed for other systems, but the origins are not fully understood. It has been proposed that the most likely explanation is damage of the fibre skin at the point where the fibre enters the matrix [18].

The solid line in *figure 4a* represents the theoretical partial debonding model [10] fitted to the data using *equation 12* to model the linear strain distribution in the debonded region and *equation 1* to model the shear-lag exponential decay in the elastically bonded region. Using the fitting parameters listed in the figure caption it is possible to attain good agreement between the theoretical and experimental data in the bonded region. In the debonded regions the gradient of the theoretical fit was optimised by using *equation 12* and adjusting the interfacial frictional shear stress, $_{frict}$; the frictional shear stress values used can be found in *figure 4b* (as described below).

The interfacial shear stress, , along the fibre was calculated by fitting the partial debonding model to the experimental data and subsequently substituting the derivative of the model curve, de_f/dx, into *equation 17*. The variation of , with x is presented in *figure 4b*. Starting from x = 0, for the theoretical curve to the right hand side of the crack plane, it can be seen that there are two regions of constant shear stress, reflecting the change in strain gradient along the debonded region of the fibre/matrix interface. The shear stress then rises sharply to a singular peak at the bonded/debonded transition, before decaying exponentially in the fully-bonded region. This is exactly the form expected for a partially-debonded fibre [10]. The values of frictional shear stress, $_{frict}$, in the debonded regions are between, 0 and 10 MPa. In the fully-bonded region $_{max}$ to the left and to the right $_{max}$ of the crack plane is ~ 36 MPa.

4.2 Zylon/epoxy

Figure 5a, shows the micromechanical strain distributions along a crack bridging Zylon fibre, at COD = 35 m. It can be seen that for the particular fibre chosen, the strain profile to the left of the crack plane is approximately similar to that to the right, as was the case for all Zylon fibres studied. The distribution of strain along the fibre is qualitatively similar to that for Twaron, hence the micromechanical deformation process during crack-bridging is similar for the different materials. The distribution of strain extending to the left and to the right, from the crack-plane, along the fibre embedded in the matrix can be seen to incorporate several regions where the distribution of strain varies linearly, with a debonded length of 2.2 mm to the left of the crack plane and 2.7 mm to the right. The strain at the end of the debonded regions on both sides of the crack plane is ~ 0.48 %.

At the end of the linear regions the transition from the debonded to the fully-bonded region is marked by the characteristic sharp change in the gradient of the strain profile in the form of exponential decay, typical of elastic strain transfer which takes place when the fibre and matrix remain bonded. The strain in the bonded region decays and tends to zero over a distance of ~ 0.5 mm.

There is good correlation between the theoretical model (shown as a solid line) and the experimental data for the Zylon epoxy system. The interfacial shear stress distributions which are derived from the theoretical strain distributions are presented in *figure 5b*. The interfacial shear stress in the debonded regions varies but is generally between -5 and 5 MPa (the sign indicates direction of stress). The shear stress at the debonded-bonded transition, $_{max}$, on both sides of the crack plane is found to be 30 - 33 MPa indicating that for the Zylon/epoxy system debonding occurs well below the shear yield stress of the matrix which is 43 MPa [8]; the interfacial shear stress decays from these points with distance x along the fibre.

4.3 T50u/epoxy

Figure 6 shows the micromechanical strain distribution along a T50u carbon fibre where matrix crack propagation has caused the fibre to break; the COD was maintained at COD = 5 m. The strain distribution indicates that the fibre is subjected to a slight residual compressive strain over an approximate distance of 0.35 mm. It can be seen that for the particular fibre chosen, the strain profile to the left of the crack plane approximately mirrors that to the right; this was the case for most carbon fibres observed.

A point with error bars, has been plotted in *figure 6*, to indicate the scatter associated with an undeformed fibre in an undeformed matrix. The error bars are based on the scatter of data from a carbon fibre embedded in an undeformed fragmentation specimen [19]. The fibre strain distribution is outside the limits of the scatter and hence the strain gradient which corresponds to a frictional shear stress of between 6 and 9 MPa (derived from the solid line fitted to the data) is real, indicating interfacial failure must have occurred during the matrix cracking process. The fibre around the crack plane is in compression probably as a result of reverse sliding caused by fibre recoil following fracture.

4.4 M5/epoxy

Figure 7 shows the micromechanical strain distribution along a broken M5 (PIPD) fibre after matrix crack propagation, at COD = 13 m. The strain distribution, indicates that the fibre is subjected to residual strain caused by the matrix cracking over a distance of approximately 0.2 mm. For the particular fibre chosen, the strain profile is slightly asymmetric.

As for carbon, a point with error bars, has been plotted in *figure 7* to indicate the scatter associated with an undeformed fibre in an undeformed matrix. The error bars are based on the scatter shown in for an M5 fibre embedded in an undeformed fragmentation sample [20]. It can be seen that the fibre strain distribution, as with T50u (above), is outside the limits of the scatter and hence represents interfacial deformation. Thus the fibre strain gradient which corresponds to a frictional shear stress of between 10 and 17 MPa (derived from the solid line fitted to the data) is real, indicating interfacial failure must have occurred during the cracking process. Again, the fibre around the crack plane is in compression probably as a result of reverse sliding caused by fibre recoil.

4.6 Fibre recoil

The evidence from the fibre strain distributions from the T50u and M5 systems shown in *figures 6* and *7* respectively, indicates that some interfacial failure has occurred. The nature of the failure, however, could not be determined as it was not possible to reload the fibres by crack opening. It can be seen that the fibre in both cases is in compression along the failed region. One possible reason for the compression could be fibre recoil along the failed region. The proposed fibre recoil process depicted schematically in *figure 8*, is envisaged to proceed as follows; (a) the fibre is stretched across an opening matrix crack, (b) just after fibre fracture there is excess strain energy stored in the fibre, (c) the fibre overshoots during the

recovery of the excess strain energy and is pinned or locked in place by the frictional constraints of the matrix.

5 SEM Investigations

5.1 Twaron/epoxy

Generally for Twaron fibres it was found that failure occurred close to the crack plane. In isolated cases, however, it has been possible to observe fibre failure away from the crack plane. This has made it possible to examine the state of the fibre surface and has help to gain some insight into the interfacial failure mechanisms occurring. *Figures 9a,b* show SEM micrographs of a broken crack-bridging Twaron fibre which has fractured some distance inside the matrix (away from the crack plane) and the matrix cavity from which it has been extracted. Examination of the fibre surface, *figure 9a*, reveals a smooth surface similar to that of the as-received Twaron fibre [16]. There is however, some evidence of fibre surface damage and it can be seen that some skin has been peeled from the fibre. There is also evidence of defibrillation of the fibre skin. These observations are supported by the corresponding micrograph of the cavity, *figure 9b*, where a sliver of skin can be seen protruding from the hole along with the fibrillated skin.

5.2 Zylon/epoxy

In the case of Zylon fibres significant lengths of fibre were pulled from the matrix during fracture. *Figure 9c & d*, shows FEGSEM micrographs of a broken crack-bridging fibre protruding from the crack face and the matrix cavity on the opposing crack face, from which it was extracted. Ultimate failure of the fibre has occurred within the matrix, resulting in a length of fibre being pulled out. Examination of the fibre at the point of exit from the matrix, *figure 9c*, shows that the fibre skin is ravelled up or kinked and that a strip or strips of skin have been torn from the fibre. Conversely, part of the surface of the fibre skin has remained relatively 'undamaged' and appears to be very smooth (not much different from an as-received fibre) [16].

5.3 T50u/epoxy

For the T50u fibre failure occurred at, or in the immediate vicinity of the crack plane. This is illustrated by *figures 9e,f*, which show SEM micrographs of a failed fibre end at the point of exit from the crack face. Here it can be seen, *figure 9c*, that a very small length of fibre protrudes from the matrix, indicating it has broken away from the crack plane and supporting our earlier observation that limited fibre matrix debonding has occurred. The length of the portion of protruding fibre can be seen to be very short, probably less than one fibre diameter. This is complemented by *figure 9f*, which shows a very shallow matrix cavity from which the short length of fibre has been extracted. The complementary fracture surface of the broken fibre can be seen inside the matrix cavity. Examination of both the fibre protruding from the crack face and the fibre in the matrix cavity at the other crack face shows the fibre to have maintained the integrity of its skin and core.

5.4 M5/epoxy

For M5 (PIPD) fibres, complete fibre failure occurred at/or around the crack plane. This is illustrated by *figures 9g,h*, which shows SEM micrographs of a failed fibre end protruding from the matrix and the cavity from which it has been extracted, respectively. *Figure 9g* shows a short length of ragged fibre extending from the matrix indicating that a certain amount of defibrillation has occurred. The length of the portion of protruding fibre can be seen to be fairly short, probably no more than a few fibre diameters. In figure *9h* some short lengths of fibre skin can be seen protruding from the matrix cavity.

5.5 Crack-tails

The 'crack-tail' takes the form of a mark or scar on the surface of the matrix crack face. In *figures 9c-h*, the micrographs for Zylon, T50u and M5 fibres show a tail running away from the fibre in the direction of crack propagation, as indicated. This phenomenon [21], indicates the matrix crack has travelled around the inclusion (fibre), hence at some point the fibre must have bridged the crack.

The mechanism which is depicted schematically in *figure 10* proceeds as follows; (a) the front of a propagating matrix crack approaches an inclusion (in this case a fibre), (b) the crack is split by the inclusion and slowed in the area around it, (c) as it passes the inclusion the crack front joints up again on different levels, (d) a tail is formed running way from the fibre in the direction of the propagating crack.

6 Discussion

For the fibre/matrix systems studied here both fibre/matrix interfacial failure and fibre fracture have been observed. While the type of fibre used has been varied, the resin matrix has been kept constant throughout and been prepared in an identical manner for all specimens.

6.1 Twaron/epoxy

Figure 11 shows the plot of $_f$* versus E_f with the boundary between fibre fracture and interfacial debonding drawn for the Twaron/epoxy system. A limiting value of $_{max}$ ~ 40 MPa was used. The data point for Twaron falls above the theoretical (solid) line indicating that when a matrix crack impinges on the fibres, the interface should fail with intact fibres bridging the faces of the crack.

However, once failure has been initiated and debonding has begun to propagate then the partial-debonding conditions must be applied. It can be seen that this moves the critical condition (dashed line) in favour of fibre fracture. The partial debonding conditions applied include a debond length of 1.2 mm. The magnitude of interfacial frictional shear stress values measured for crack bridging Twaron fibres ranges between 0-10 MPa, therefore a value of 5 MPa was chosen for the purposes of this model. For these conditions it can be seen that the data point is fairly close to the boundary, indicating that debonding > 1.2 mm will be limited by a critical build up of stress in the debonded zone and will cause fibre fracture to occur across the crack plane.

6.2 Zylon/epoxy

Figure 12 shows a comparison between the tensile strength and modulus components of a Zylon fibre and the theoretical boundary conditions for this system. The plot of $_f^*$ versus $E_f^{1/2}$, *figure 12*, with the boundary between fibre fracture and interfacial debonding shows that the data point for Zylon falls well above the theoretical line indicating when a matrix crack impinges on the fibres, the interface should fail with intact fibres bridging the faces of the crack.

It can be seen in *figure 12* that when typical partial debonding conditions for this fibre are applied, at a debond length of 3 mm and an interfacial frictional shear stress of 3 MPa, that the model predicts the Zylon fibre remains intact bridging the faces of the crack. The point for Zylon still lies a considerable distance above the line. This can be attributed to its

exceptional strength (4.9 GPa). Thus it is inferred from the model that it would take a considerable increase in the interface strength, the debond length or the interfacial frictional shear stress to cause fibre fracture, which did not occur in this case.

6.3 T50u/epoxy

Figure 13 shows the plot of $_f$* versus $E_f^{1/2}$, with the boundary between fibre fracture and interfacial debonding drawn for T50u carbon fibres embedded in the epoxy resin matrix. Stress transfer information for this system was not directly measurable by crack-bridging experiments because stable bridging did not occur, therefore the data from fragmentation experiments using Raman spectroscopy [19] were used. The maximum interfacial strength of the system was estimated to be ~27 GPa. The modulus, E_f, of T50u has been measured at 324 GPa and its tensile strength at 2.27 GPa. It can be seen for the initiation of interfacial failure the data point for T50u falls just above the theoretical curve (solid line) indicating that when a matrix crack impinges on the fibres, the interface is likely to fail with intact fibres bridging the faces of the crack. Raman experiments on the T50u/epoxy system confirmed that some limited interfacial failure does occur over an approximate distance of 0.35 mm, however the fibres were also found to have fractured.

An explanation for the observation of both interfacial failure and fibre fracture can be arrived at by considering the partial-debonding aspect of the strength criterion. When the partial debonding conditions, *figure 13*, are applied (dashed line) for a debond length of 0.35 mm, typical for this system, it can be seen that there is good correlation between the data point for carbon fibre and the boundary conditions. Two factors are critical in the correlation between the actual data of the theoretical boundary conditions. Firstly, the interfacial frictional shear stress, $_{frict}$ = 8 MPa, which was the maximum value observed by fragmentation studies [20], is higher than the values used for Twaron and Zylon thus the rate of build up of fibre stress by transfer along the frictional interface is greater. Secondly the fibre radius, r = 3.6 m, is significantly smaller than those of Twaron and Zylon. It can be seen from *figure 3d* that this has a significant effect on the critical conditions for debonding/fibre fracture.

6.4 M5/epoxy

Figure 14 shows the plot of $_f$* versus $E_f^{1/2}$, marking the critical condition between fibre fracture and interfacial debonding drawn for a M5/epoxy, fibre/matrix system with $_{max}$ as the shear yield stress of 43 MPa. Due to fibre fracture, relevant stress transfer data for M5 was not obtainable directly from crack-bridging experiments and was obtained from fragmentation data obtained in an earlier study [21]. The data point for M5 is above the theoretical curve (solid line) indicating when a matrix crack impinges on the fibres, the interface is likely to fail with intact fibres bridging the faces of the crack. In common with T50u fibres, Raman experiments on the M5/epoxy system confirm, even though the fibres were also found to have fractured, that some limited interfacial failure does occur over an approximate distance of 0.3 mm.

It can be seen that although the system easily satisfies the condition for initial debonding that when the partial debonding conditions, *figure 11*, are introduced (dashed line) using a typical debond length of 0.3 mm and $_{frict}$ = 25 MPa [21] there is good correlation between the model and the data. The relatively high interfacial frictional shear stress appears to be a critical factor, causing the stress in the fibre to build up to the fibre failure stress over a very short debond length.

6.5 Fibre/interface properties and crack bridging

Table 3 presents a summary of the various properties relating to the fibre, the interface and the crack bridging behaviour of the various fibre/matrix systems studied. It is indicated, which fibres form a stable bridge across the matrix crack (i.e. without fibre fracture) with significant interfacial debonding and which fibres fracture with relatively little interfacial failure. From the model it is possible to make some observations about the crack bridging behaviour of the fibres in relation to the data presented in *table 3*.

Predictions from the strength criterion indicated that all the fibres studied were strong enough to remain intact such that interfacial debonding would occur as a result of matrix cracking. The results obtained from the crack bridging experiments showed that while Twaron fibres formed a stable bridge across the crack with interfacial debonding occurring over distances > 1 mm, T50u fibres which have a similar strength were found to fracture with very little interfacial debonding, ~ 0.35 mm. M5 fibres, which are substantially stronger than both Twaron and T50u also fractured with very little interfacial failure. Zylon fibres which have an exceptionally high strength (much greater than the other fibres) were shown to form a very stable bridge and were found to debond over distances > 2 mm.

In the case of T50u, which has the highest modulus of all the fibres, it can be seen from *figure 13* that the higher the fibre modulus then the more likely it is that conditions will favour fibre fracture. Secondly T50u has a much smaller radius than the other fibres, hence when the debonding criterion is applied, decreasing the fibre radius will shift the critical condition in favour of fibre fracture.

The explanation for fibre fracture in the case of M5 is different from that of T50u. The fragmentation experiments have shown [21] that the M5/epoxy system has a comparatively high interfacial frictional shear stress after fibre matrix debonding, hence causing the stress in the fibre to build up to the fibre strength over a very short debond length. Thus it appears that in this case the interfacial frictional shear stress is the critical factor.

7 Conclusions

The comparison between the modulus and tensile strength data for the various fibre matrix systems studied and the boundary conditions drawn according to the theoretical strength criterion correlate well with experimental data obtained from the Raman experiments. Since Twaron and Zylon are tough fibres that remain intact after matrix cracking, it is shown that after initial failure of the fibre/matrix interface, considerable debond propagation is possible. In the cases of T50u and M5 fibres, however, although initial debonding is possible, the fibre properties and the interfacial failure characteristics limit debonding to much smaller lengths.

The effects of frictional stress transfer in the debonded region and fibre radius are very important in determining the rate of build up of stress in the fibre and thus will be crucial in determination of a maximum possible debond length, limiting interfacial failure before fibre fracture. As the level of frictional shear stress, $_{frict}$, increases then the debond length decreases before fibre fracture occurs. When all of the other material parameters are kept constant, a greater toughening effect is to be had by increasing the fibre strength. Conversely this effect is reversed by an increase in fibre modulus.

Although this present study has been confined to model single fibre composite systems, it has important implications for the behaviour of fibre-reinforced composites in general. It is anticipated that the similar factors such as the balance between interfacial shear strength, fibre strength and the physical properties of the component materials will control the fracture characteristics and toughening behaviour of high volume fraction composite systems.

Acknowledgments

The authors would like to extend thanks to the EPSRC who funded this work (Grant number EP/C002164/1).

References

1. Chawla, K K, *Ceramic Matrix Composites,* 1st edition, Chapman and Hall, London, 1993.
2. Piggott M R, *Load Bearing Composites*, Pergamon Press, Oxford, UK 1980. p.83-89.
3. Hull D, *An Introduction to Composite Materials*, Cambridge University Press, 1981. p.137.
4. He M Y, Hutchinson J W, Crack deflection at an interface between dissimilar elastic materials, *Int. J. Solids and Structures,* 1989;9:1053-1067.
5. Bennett J A, Young R J, Micromechanical aspects of fibre/crack interaction in an aramid/epoxy composite, *Composites Part A: Applied Science and Manufacturing,* 1998;29:1071-1081.
6. Bannister D J, Andrews M C, Cervenka A J, Young R J, Analysis of the single fibre pull-out test by means of Raman spectroscopy: Part II. Micromechanics of deformation for an aramid/epoxy system, *Comp. Sci. & Technol.*, 1995;53**:**411-421.
7. Andrews M C, Day R J, Hu X, Young R J, Deformation micromechanics in high-modulus fibres and composites, *Comp. Sci. & Technol.,* 1993;48:255-261.
8. Andrews M C, Young R J, Analysis of the deformation of aramid fibres and composites using Raman spectroscopy, *J. Raman Spectroscopy*, 1993;24**:**539-544.
9. Young R J, Andrews M C, Deformation micromechanics in high-performance polymer fibres and composites, *Mater. Sci. & Engng.* 1994;A184:197-205.
10. Piggott M R, Micromechanics of fibre-polymer interfaces. In *Interfacial Phenomena in Composite Materials*, ed. Verpoest I, & Jones F R, Butterworth Heinemann, Oxford, UK, 1991. p. 2-8.
11. Cox H L, The elasticity and strength of paper and other fibrous materials, *British Journal of Applied Physics*, 1952;3:72-79.
12. Nairn, J A, On the use of shear-lag methods for analysis of stress transfer in unidirectional composites. *Mechanics of Materials*, 1997;26:63-80.
13. Nayfeh A H, Thermodynamically induced interfacial stresses in fibrous composites. *Fibre Sci. & Tech*. 1977;10:195-209.
14. McCartney, L N, New theoretical model of stress transfer between fibre and matrix in a uniaxially fibre-reinforced composite. *Proc. R. Soc. London A* 1989;425:215-244.
15. Cervenka A J, Young R J, Kueseng K, Micromechanical phenomena during hygrothermal ageing of model composites investigated by Raman spectroscopy. Part

II: comparison of the behaviour of PBO and M5 fibres compared with Twaron *Composites Part A: App. Sci. & Man.* 2005;36:1020-1026.

16. Kelly A, McMillan N H, Strong Solids, Clarendon Press, Oxford, 1986.
17. Bennett J A, Fibre/Crack Interaction in Polymer Matrix Composites, PhD Thesis, UMIST, Manchester, UK, 1998.
18. Marotzke C, The elastic stress field arising in the single fibre pull-out test, *Comp. Sci. & Tech.*, 1994;50:393-405.
19. Yallee R, Single fibre composite micromechanics for alpha-alumina and carbon/epoxy systems, PhD Thesis, UMIST, Manchester, UK, 1997.
20. So C L, Bennett J A, Sirichaisit J, Young R J, Compressive behaviour of rigid rod polymer fibres and their adhesion to composite matrices, *Plast. Rub. & Comp.*, 2003;32:199-205.
21. Kinloch A J, Young, R J, *Fracture Behaviour of Polymers*, Applied Science, London, 1983.

Table 1 Mechanical properties of Twaron, Zylon, T50u and M5 fibres; determined from single fibre specimens of 50 mm gauge length.

Fibre	E_f **(GPa)**	$_f$*** (GPa)**	e_f*** (%)**	r **(m)**
Twaron	104 4	2.1 0.2	2 0.1	12.4 0.3
Zylon	228 16	4.9 0.5	2.1 0.2	13.5 1
T50u	320 26	2.3 0.4	0.7 0.1	7.2 0.3
M5	304 17	3.7 0.3	1.6 0.2	13.4 0.8

Table 2 Raman band shift rates for Twaron, Zylon, T50u and M5 fibres; obtained from single fibres in air [14].

Fibre	Strain sensitive band (cm^{-1})	d /de_f, (cm^{-1})/%
Twaron	1610	3.7 0.3
Zylon	1618	5.5 0.4
T50u	1580	12.5 0.5
M5	1615	15.3 0.3

Table 3 Fibre, interfacial shear stress and crack bridging properties of Twaron, Zylon, T50u and M5 fibres

Fibre	E_f (GPa)	$_f$* (GPa)	$_{max}$ (MPa)	$_f$ (MPa)	r (m)	L_d (mm)	Stable bridge
Twaron	104	2.1	33	0-10	6.2	1.2	✓
Zylon	228	4.9	33	0-5	6.75	> 2	✓
T50u	325	2.3	27	8	3.6	0.35	×
M5	304	3.7	40	20	6.7	0.3	×

Figure Captions

Figure 1 Dependence of fibre fracture/interfacial debonding upon the relationship between fibre strength, $_f^*$, and fibre modulus E_f with (a) variation in interfacial shear strength, $_{max}$, and (b) variation in matrix modulus E_m. Except where given, the relevant physical properties used were as follows: E_m = 3 GPa, $_{max}$ = 40 GPa, $_m$ = 0.35, n = 0.1.

Figure 2 Dependence of fibre fracture/interfacial debonding upon the relationship between fibre strength, $_f^*$, and fibre modulus E_f with (a) increasing debond length, L_d, and (b) variation in interfacial frictional shear stress, $_{frict}$, in the failed/debonded region. Except where given, the relevant physical properties used were as follows: E_m = 3 GPa, $_{max}$ = 40 GPa, $_m$ = 0.35, n = 0.1, L_d = 0.2 mm, r = 6.25 m, $_{frict}$ = 8 MPa.

Figure 3 Schematic representation of a crack-bridging fibre in a CCT specimen

Figure 4 Distribution of (a) fibre strain, e_f, the relevant physical properties for the partial-debonding model (solid line) were as follows: E_f = 105 GPa, E_m = 3 GPa, $_m$ = 0.35, n = 0.1, r = 6.25 m; and (b) the distribution of interfacial shear stress, , along an unbroken, loaded, crack-bridging Twaron fibre in an epoxy resin matrix

Figure 5 Distribution of (a) fibre strain, e_f, the relevant physical properties for the partial-debonding model (solid line) were as follows: E_f = 228 GPa, E_m = 3 GPa, $_m$ = 0.35, n = 0.07, r = 6.25 m; and (b) distribution of interfacial shear stress, , along an unbroken, loaded, crack-bridging Zylon fibre in an epoxy resin matrix

Figure 6 Distribution of (a) fibre strain, e_f, and (b) distribution of interfacial shear stress, , along a broken, loaded, crack-bridging T50u fibre in an epoxy resin matrix

Figure 7 Distribution of (a) fibre strain, e_f, and (b) distribution of interfacial shear stress, , along a broken, crack-bridging M5 fibre in an epoxy resin matrix

Figure 8 Schematic representation of a fibre (a) bridging a crack, (b) just after fibre fracture and (c) recoiling into the matrix cavity.

Figure 9 SEM Micrographs showing corresponding pairs of fractured (a,b) Twaron, (c,d) Zylon, (e,f) T50u and (g,h) M5 fibres at the matrix crack plane.

Figure 10 Schematic illustration of a crack front (a) approaching a fibre, (b) splitting and slowing, (c) rejoining and (d) forming a tail.

Figure 11 Comparison of the relationship between fracture strength, $_{f}^{*}$ and fibre modulus, E_f, with the boundary conditions for fibre fracture/interfacial failure in an Twaron fibre/epoxy composite material.

Figure 12 Comparison of the relationship between fracture strength, $_{f}^{*}$ and fibre modulus, E_f, with the boundary conditions for fibre fracture/interfacial failure in a Zylon fibre/epoxy composite material.

Figure 13 Comparison of the relationship between fracture strength, $_{f}^{*}$ and fibre modulus, E_f, with the boundary conditions for fibre fracture/interfacial failure in a T50u-carbon fibre/epoxy composite material.

Figure 14 Comparison of the relationship between fracture strength, $_{f}^{*}$ and fibre modulus, E_f, with the boundary conditions for fibre fracture/interfacial failure in a M5-PIPD fibre/epoxy composite material.

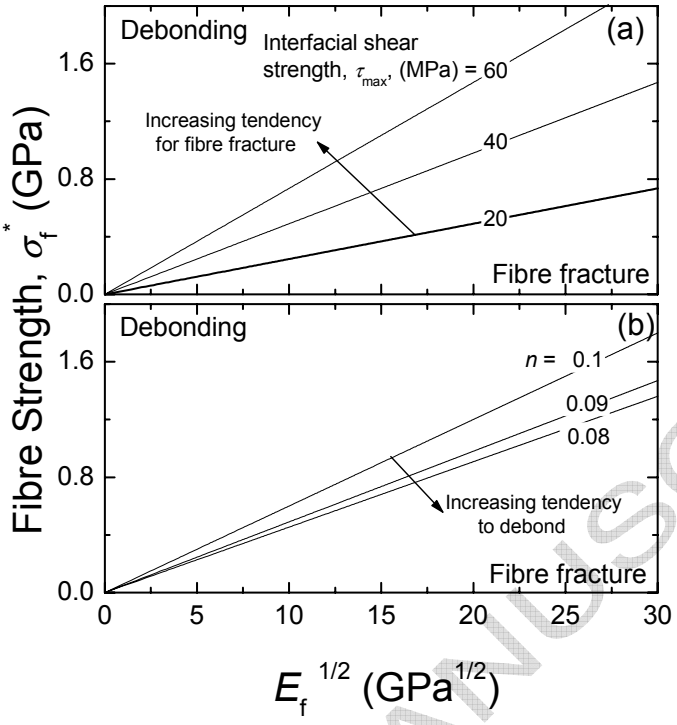

Figure 1

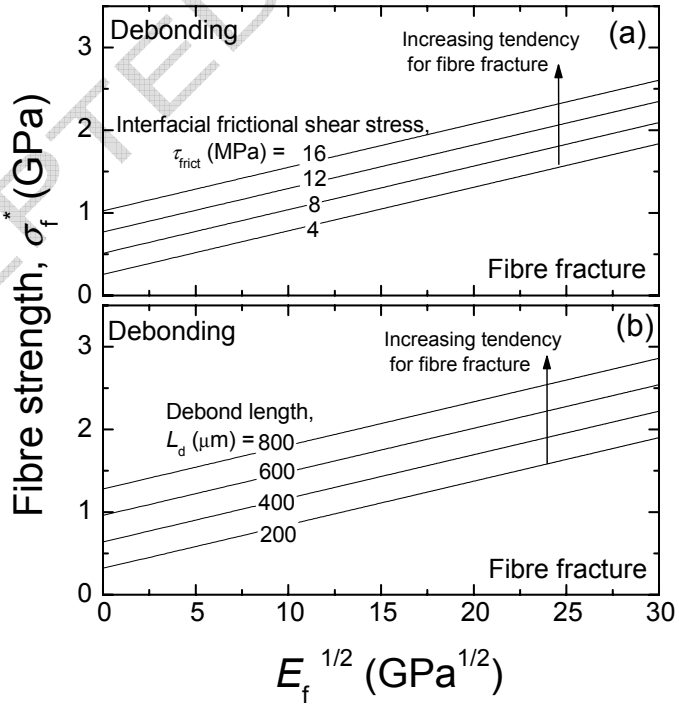

Figure 2

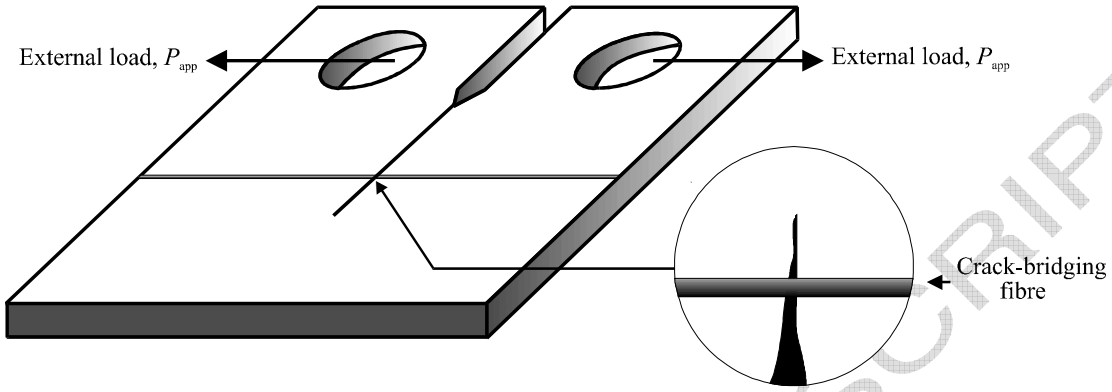

Figure 3

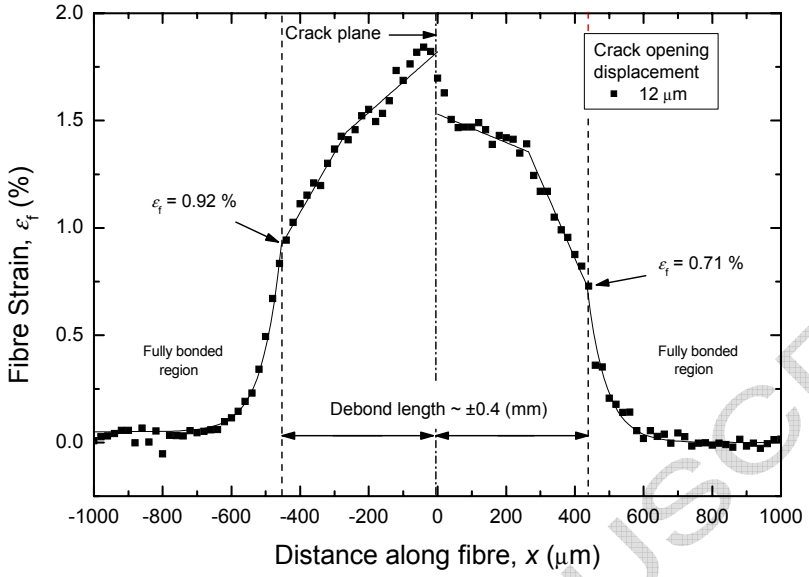

Figure 4a

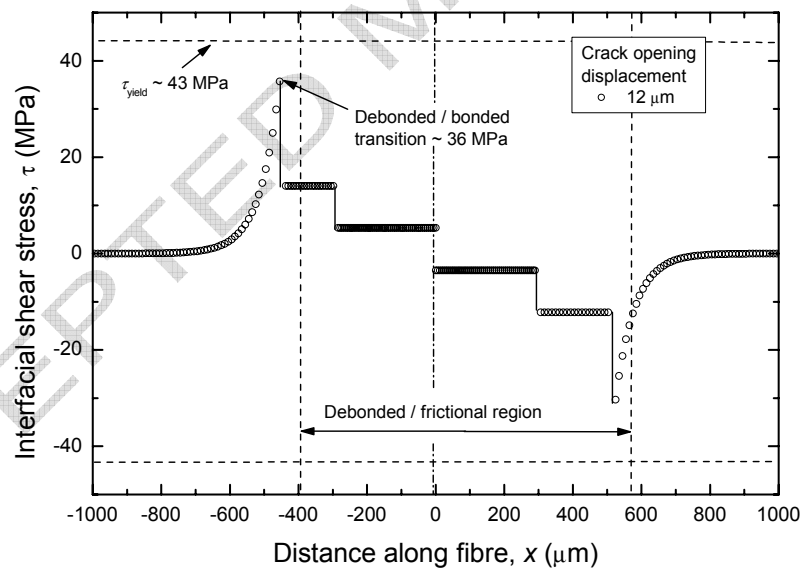

Figure 4b

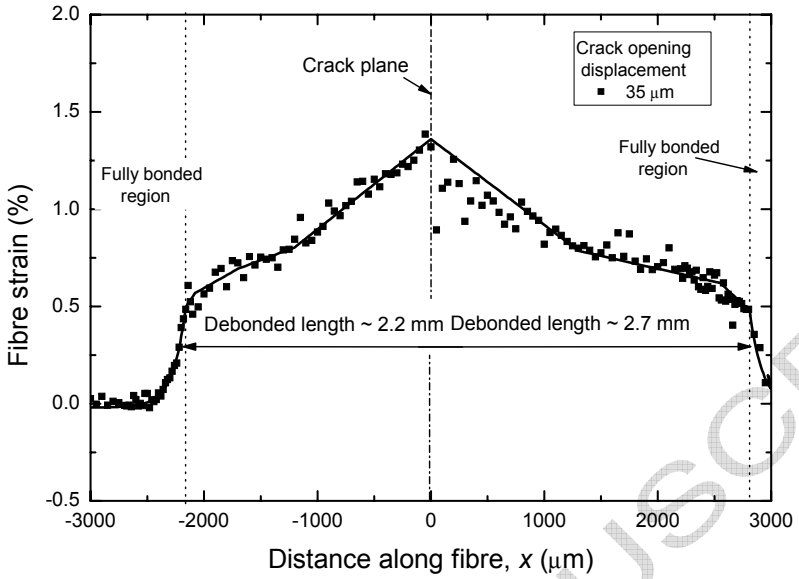

Figure 5a

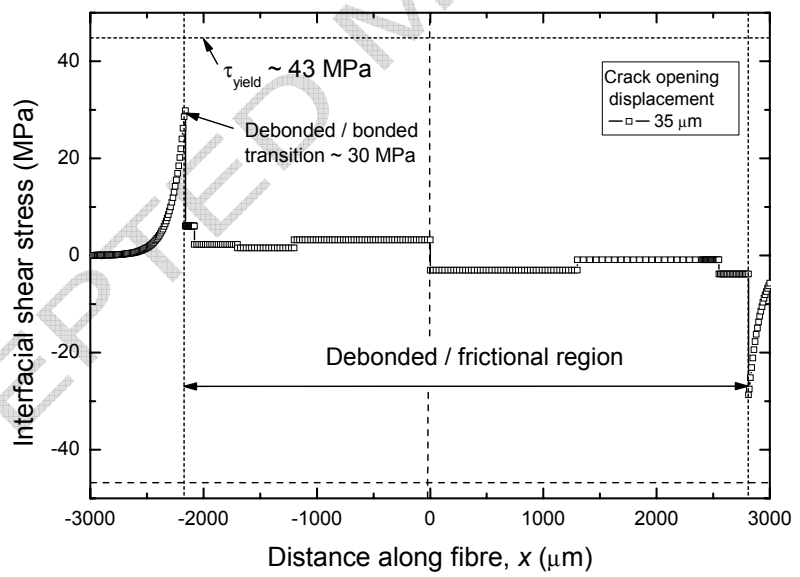

Figure 5b

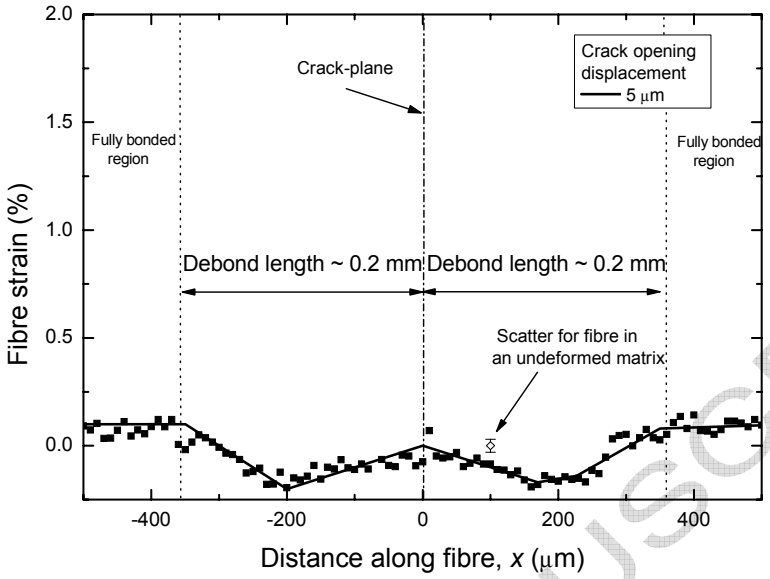

Figure 6

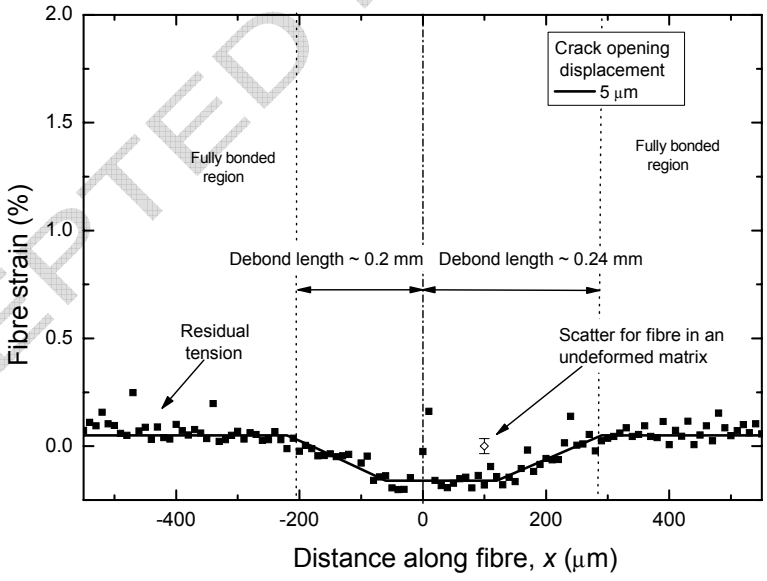

Figure 7

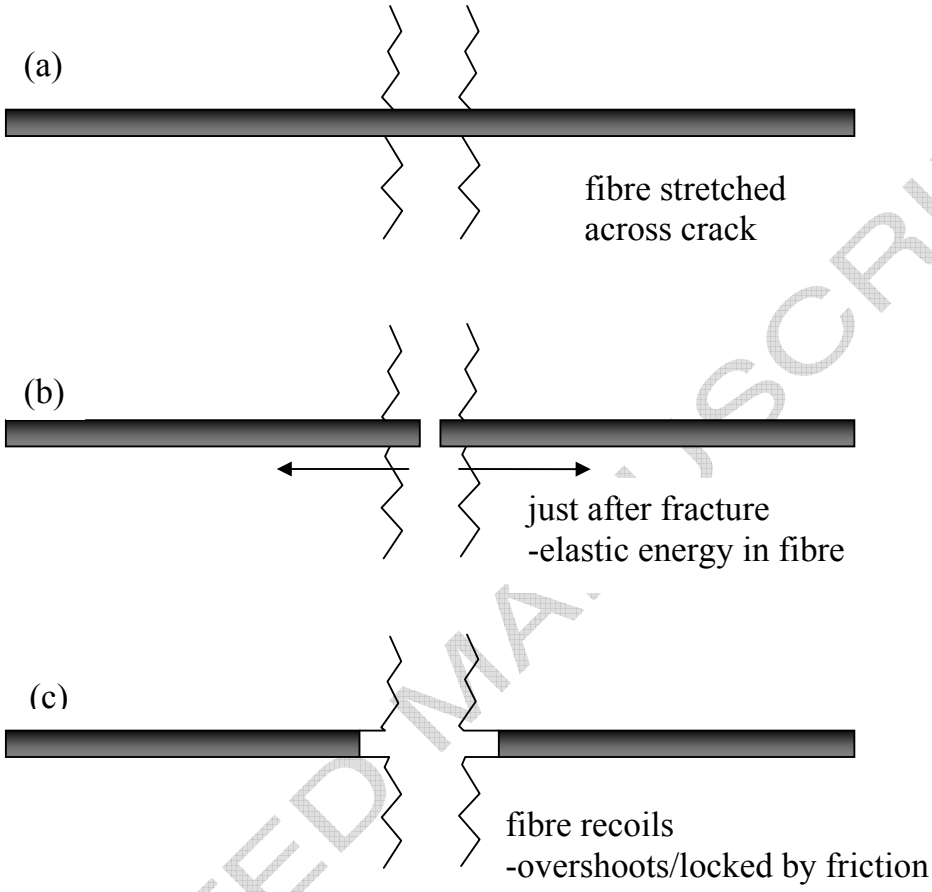

Figure 8

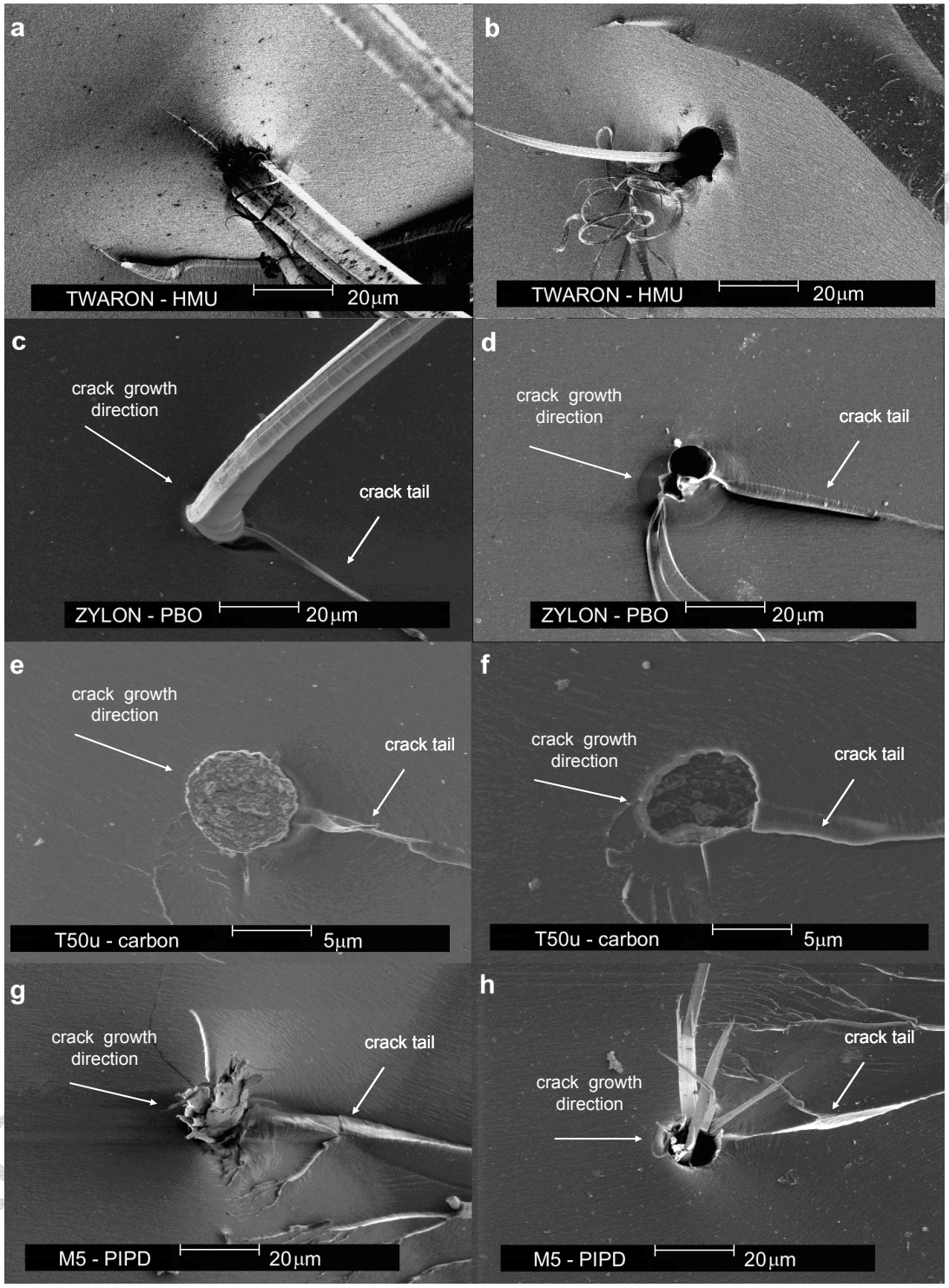
a
TWARON - HMU
20μm
b
TWARON - HMU
20μm
c
crack growth direction
crack tail
ZYLON - PBO
20μm
d
crack growth direction
crack tail
ZYLON - PBO
20μm
e
crack growth direction
crack tail
T50u - carbon
5μm
f
crack growth direction
crack tail
T50u - carbon
5μm
g
crack growth direction
crack tail
M5 - PIPD
20μm
h
crack growth direction
crack tail
M5 - PIPD
20μm

Figure 9

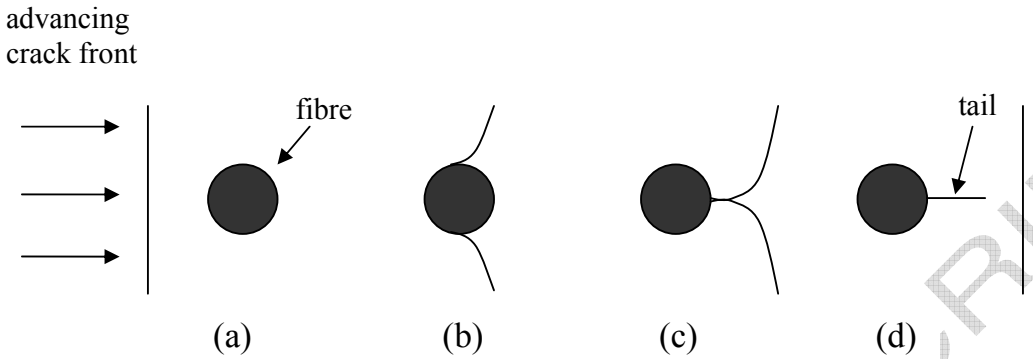

Figure 10

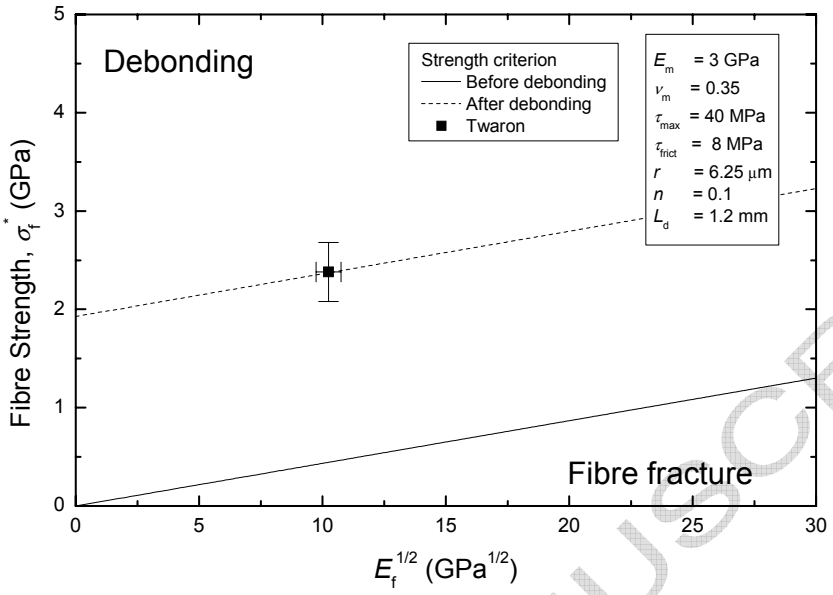

Figure 11

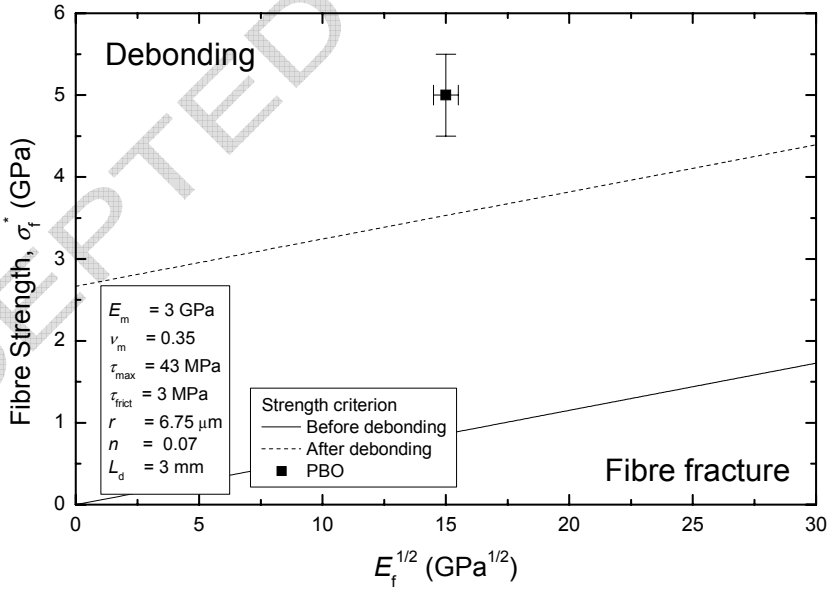

Figure 12

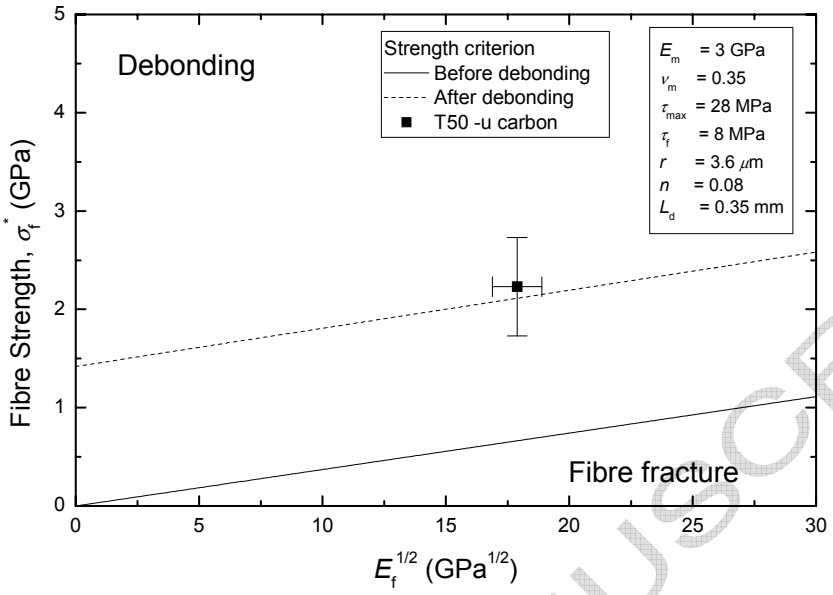

Figure 13

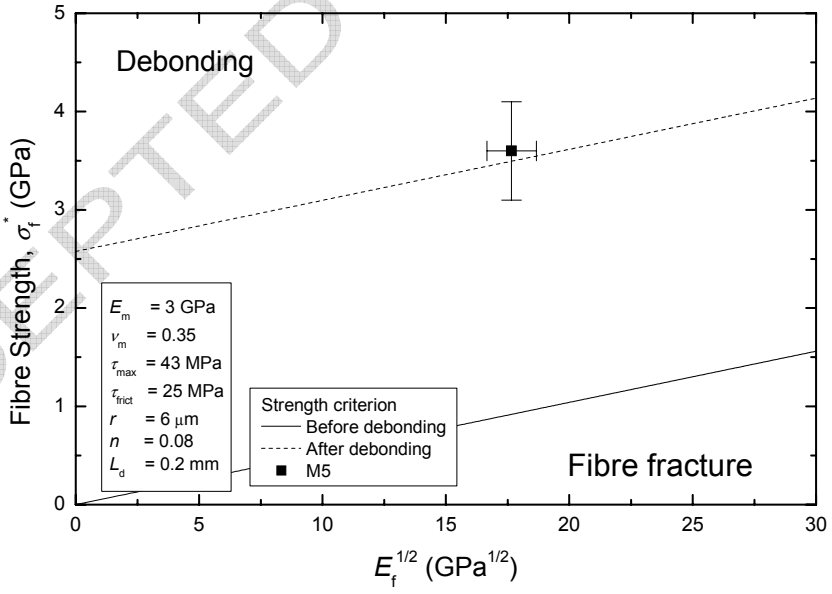

Figure 14